

PAPER • OPEN ACCESS

Exploring nanowire regrowth for the integration of bottom-up grown silicon nanowires into AFM scanning probes

To cite this article: A Behroudj *et al* 2021 *J. Micromech. Microeng.* **31** 055010

View the [article online](#) for updates and enhancements.

You may also like

- [Silicon nanowires: the promoter of performance improvement of microplasma in a microcavity array device](#)
Xiaoqin Ma, Yaogong Wang, Lichi Chen et al.
- [Structural and photoluminescence properties of silicon nanowires extracted by means of a centrifugation process from plasma torch synthesized silicon nanopowder](#)
Vincent Le Borgne, Marta Agati, Simona Boninelli et al.
- [Conductive and Porous Silicon Nanowire Anodes for Lithium Ion Batteries](#)
Chihyun Hwang, Kangmin Lee, Han-Don Um et al.

Exploring nanowire regrowth for the integration of bottom-up grown silicon nanowires into AFM scanning probes

A Behroudj¹, P Salimitari², M Nilsen¹  and S Strehle^{2,*} 

¹ Ulm University, Institute of Electron Devices and Circuits, Albert-Einstein-Allee 45, 89081 Ulm, Germany

² Technische Universität Ilmenau, Institute of Micro- and Nanotechnologies MacroNano[®], Microsystems Technology Group, Max-Planck-Ring 12, 98693 Ilmenau, Germany

E-mail: steffen.strehle@tu-ilmenau.de

Received 4 January 2021, revised 6 March 2021

Accepted for publication 29 March 2021

Published 13 April 2021



CrossMark

Abstract

Bottom-up grown single-crystalline silicon nanowires (SiNWs) are highly intriguing to build nanoscale probes, for instance for atomic force microscopy (AFM), due to their mechanical robustness and high aspect ratio geometry. Several strategies to build such nanowire-equipped probes were explored but their fabrication is still elaborate, time-consuming and relies partly on single-crystalline substrates. Here, we explore a new strategy to fabricate AFM probes that are equipped with single-SiNW scanning tips. The conceptual evaluation begins with a discussion on the overall design and softness of such probes based on finite-element-method simulations. For the experimental realization, SiNWs were grown by the well-established gold-catalyzed vapor–liquid–solid method employing gaseous monosilane. As-grown SiNWs were subsequently transferred onto flexible membranes and even freestanding AFM microcantilever beams via mechanical nanowire contact printing. Elongation of the deposited nanowires by so-called regrowth was triggered by reusing the original gold catalyst to yield the prospective AFM scanning tip. SiNW-equipped scanning probes were created in this manner and were successfully employed for topography imaging. Although a multitude of challenges remains, the created probes showed an overall convincing performance and a superior durability.

Supplementary material for this article is available [online](#)

Keywords: nanowire, silicon, AFM, soft probe, microfabrication, nanowire alignment

(Some figures may appear in color only in the online journal)

1. Introduction

Atomic force microscopy (AFM) represents a well-established nanoanalytic technique, whose applications range from plain topographical surface reconstruction, over mechanical and

electrical sample characterizations to measurements in liquids and even on living cells [1–5]. The key element for AFM is the scanning probe itself, commonly represented by a microcantilever beam equipped with a pyramidal scanning tip. When the tip comes into close proximity to a sample surface, surface force interactions deflect, for instance, the beam and create thus a signal, e.g. for topography reconstruction [6, 7]. The achievable resolution relies naturally on the tip radius, but also on the overall tip geometry and the operation mode. Generally, the smaller the tip radius, the higher the image resolution [8]. Conventionally employed AFM pyramid-shaped silicon tips enable already sub-nanometer resolution, but mainly on

* Author to whom any correspondence should be addressed.



Original content from this work may be used under the terms of the [Creative Commons Attribution 4.0 licence](#). Any further distribution of this work must maintain attribution to the author(s) and the title of the work, journal citation and DOI.

planar surfaces. Due to the pyramidal shape, narrow and deep trenches can hardly be imaged. Here, sharp high aspect ratio probes would excel but often suffer from wear, for instance, due to crashes of the nanoscale tip with the sample surface. Therefore, nanowires and nanotubes moved into the research focus as high aspect ratio structures [9–13]. Besides their plain geometry, the robustness and durability of nanowire scanning probes are crucial, too. Engstrom *et al* [14] compared, for instance, the performance of silicon nanowire (SiNW) and carbon nanotube based scanning tips. Although both tips outperformed pyramid-shaped tips, SiNW tips provided overall more consistency within individual measurements. This was attributed to a deteriorated Young's modulus of multi-walled carbon nanotubes triggered by defects, interlayer sliding and hollow internal structures. Such issues do not exist for single-crystalline SiNWs [14].

Here, we focus solely on bottom-up grown, single-crystalline SiNW scanning tips, due to the aforementioned advantages, their inherent property of ideal elastic deformation, and due to the technological possibilities in our research lab. An intriguing feature of a single-crystalline SiNW-based scanning tip is its ability to undergo elastic deformation whenever a certain force load is exceeded. Such a feature of elastic bending and buckling yields potentially a so-called soft tip in contrary to pyramid-shaped probes. Soft tips are highly desirable for the scanning inspection of soft and delicate samples, such as living cells and polymers, to avoid any deterioration [14, 15]. Based on the nanowire geometry and the single-crystalline nature of bottom-up grown SiNWs, breakage during elastic deformation is unlikely, which assures in principle a high durability of a SiNW scanning tip.

We show later that a SiNW tip can even survive a crash with a hard sample surface represented here by sapphire. Last but not least, gold-catalyzed SiNWs, as used here, carry the gold catalyst nanoparticle at their tip if not removed, as realized in this study, by an etching procedure (see supplementary information (available online at stacks.iop.org/JMM/31/055010/mmedia)). This aspect might be in particular interesting for tip-enhanced Raman spectroscopy (TERS) by directly exploiting the gold catalyst at the nanowire tip. The fabrication of TERS-AFM tips relies so far on sophisticated microfabrication techniques [16–18]. A hemispherical tip with a radius of 20–50 nm instead of less than 10 nm may also be advantageous for inspecting soft and delicate surfaces, but with consideration of reduced lateral resolution. The fabrication of SiNW scanning probes can in principle be realized by utilizing either top-down [19, 20] or bottom-up SiNW growth strategies [21, 22]. Regardless of the chosen nanotechnological branch, SiNW integration remains elaborate. Within a top-down fabrication scheme, nanowires would be etched out of a bulk material, which is realizable, but simultaneously challenging considering a target diameter in the range of 100 nm and below as well as an intended SiNW length of typically some microns. The alternative strategy is SiNW bottom-up growth. Bottom-up SiNW synthesis can be realized, as done here, by the well-established vapor–liquid–solid (VLS) growth [23, 24]. VLS growth relies intrinsically on metal catalysts, such as Au [23],

Al [25], and Ag [26] that yield single-crystalline SiNWs and enable control of the SiNW diameter as well as axial properties, such as doping profiles [27, 28]. However, this technique comes naturally along with the challenge of single-nanowire positioning and upright nanowire alignment. Upright alignment is achievable by initiating an epitaxial SiNW growth on $\langle 111 \rangle$ oriented single-crystalline silicon substrates. However, $\langle 100 \rangle$ oriented single crystalline wafers are often used for microcantilever fabrication, and epitaxial growth requires prior removal of the native silicon oxide and dedicated process guidance to enable epitaxial SiNW growth. We showed recently a possibility to realize epitaxial growth of SiNWs despite a presence of a native silicon-oxide [29]. Nevertheless, other microcantilever materials are also of interest, if for instance, electrical insulation, transparency or certain mechanical properties are required. Silicon nitride, for example, is of interest in this context. The key challenge for the fabrication of a single, three dimensionally oriented and localized SiNW is however the nanoscale confinement of the catalyst particle, which demands, for instance, complex and high-cost electron beam lithography or focused ion or electron beam induced deposition of the catalyst material [10, 30, 31]. A simple but capable technique for the catalyst deposition and confinement was shown by Engstrom *et al* [14] by implementing so-called stencil masks in combination with an evaporated catalyst material.

With this in mind, we aimed to explore another microfabrication strategy for an integration of VLS-grown single-SiNWs as soft scanning tips that can be realized without an inherent need to employ single-crystalline-silicon substrates within the microcantilever fabrication. The overall strategy is illustrated in figure 1(a). First, as-grown SiNWs are transferred to so-called device membranes or even directly onto microcantilever beams by nanowire contact printing (called CP in the following) [32]. In this method, SiNWs are transferred from their original growth substrate to a target substrate by frictional forces that occur as part of an induced mechanical shear motion between the two substrates. The nanowires break off from their growth substrate when a critical frictional force occurs and are deposited on the target substrate parallel to the shear direction.

To position single-SiNWs locally, so-called nanowire catchers can be utilized within a CP strategy as described in [32]. This feature was here so far omitted for simplification reasons. Notably, the transferred SiNWs possess still their metal-catalyst particle at the tip. This catalyst particle shares an interface with a single-crystalline silicon substrate, represented by the SiNW cross-section itself, which we exploited here for VLS-based SiNW elongation. This elongation is further referred to nanowire regrowth. The underlying working hypothesis was that regrowth yields a controlled nanowire kinking similar to [33–35] by initiating an epitaxial relation between the transferred SiNW cross-section and the regrown SiNW. A SiNW growing at a defined angle away from the original surface would be the result. Kinking of SiNWs is a well-studied effect in the field of nanowires. In the case of SiNWs, the nanowire grows as a single-crystalline rod with a catalyst present at its tip. If the growth process is disturbed, e.g. by a

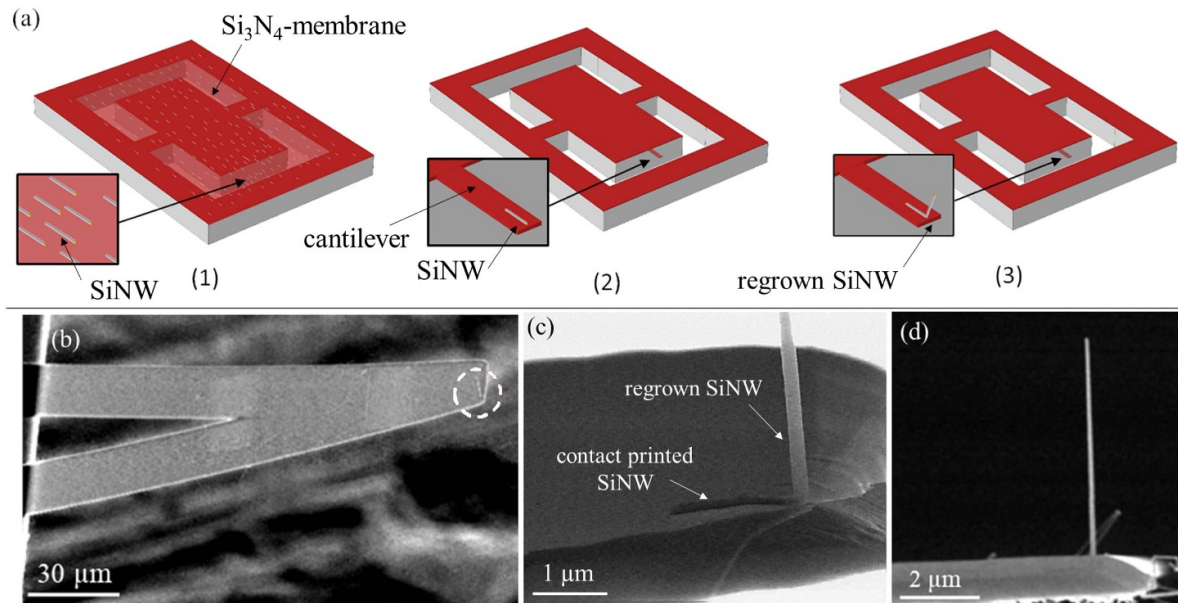


Figure 1. (a) Schematic illustration of SiNW AFM probe assembly using Si_3N_4 -membranes: (1) CP SiNWs onto the Si_3N_4 -membrane; (2) fabrication of the microcantilever; (3) SiNW regrowth on the microcantilever. (b) SEM image of a V-shaped, $1\ \mu\text{m}$ thick Si_3N_4 -microcantilever (stiffness about $0.6\ \text{N m}^{-1}$) with indicated regrown SiNW tip. (c) Magnified image of the same regrown SiNW. (d) Regrown SiNW prior to scanning usage (SEM image). The diameter and length of the regrown SiNW shown here is $120\ \text{nm}$ and $8\ \mu\text{m}$, respectively.

growth interruption or a rapid change in process parameters, the liquid catalyst droplet on the tip of the SiNW may shift. This could favor another competing crystal facet to grow further on the SiNW, resulting in kinking with a specific angle of the SiNW but without disruption of the crystal lattice. For instance, a kinking angle of 90° was reported to be formed between $\langle 112 \rangle$ and $\langle 111 \rangle$ growth directions of SiNWs [35]. Such a kinking angle is particularly interesting for our SiNW regrowth and realization of a scanning tips.

The diameter of the regrown nanowire is still controlled by the diameter of the originally transferred SiNW while the length is again controlled by the overall process parameters (e.g. gas concentration and temperature) and naturally, by the growth time. Furthermore, by assuming that the transferred SiNW adheres sufficiently strong to the microcantilever surface, the regrown SiNW can be implemented as a soft high-aspect-ratio SiNW nanoscale scanning probe.

In the following, we will discuss at first general design aspects of such SiNW scanning probes and elucidate geometric parameters that justify the term ‘soft probe’. From this discussion, it will become evident that aside from the nanowire geometry, also the mechanical properties of the cantilever must be considered. We will subsequently show that regrowth of SiNWs suffices to create SiNW scanning probes although the yield, the geometric control, and the process reproducibility require still major improvements. Nevertheless, the first successful AFM surface topography reconstructions were already realized and the SiNW scanning tips showed a superior durability, which fosters the use of such nanoscale probes in general. Further details of our experiments are given in the supplementary information file.

2. Design aspects of SiNW-equipped AFM scanning probes

To obtain an enhanced understanding of the general behavior of a vertically aligned SiNW that is attached to a microcantilever beam, finite element method (FEM) based simulations were employed (using COMSOL Multiphysics 5.3a). The SiNW was modeled in an approximation as a cylindrical object that is aligned normal to the surface of the microcantilever in its non-deformed initial state (cf figure 1(a)). The simulated probe (e.g. microcantilever surface in the force-free state) was furthermore tilted by about 12° to account for a typical AFM configuration with respect to the probe tilt. Nevertheless, note that the presented FEM simulations here only serve the purpose of elucidating the general cornerstones of SiNW-equipped AFM probes due to the lack of experimental values. Young’s modulus of silicon for thin films and nanowires has been a debatable topic for decades and is reported often to differ from the bulk value. There are numerous values for the Young’s modulus of SiNWs, determined either by simulations or experiments [36–38]. One of the reasons for the variations can arise from varying surface properties and their growing impact with progressing miniaturization [39]. In this work, a Young’s modulus for SiNWs of $170\ \text{GPa}$ was assumed based on the findings and discussion from Gordon *et al* [40] and Heidelberg *et al* [41]. Apart from the elastic modulus, all other parameters of the SiNW simulation were adopted from bulk silicon (Poisson’s ratio and density were 0.28 and $2329\ \text{kg m}^{-3}$, respectively).

The mechanical behavior of SiNWs depends intrinsically on the SiNW length and the cross-section following the bending beam theory. However, another factor that contributes

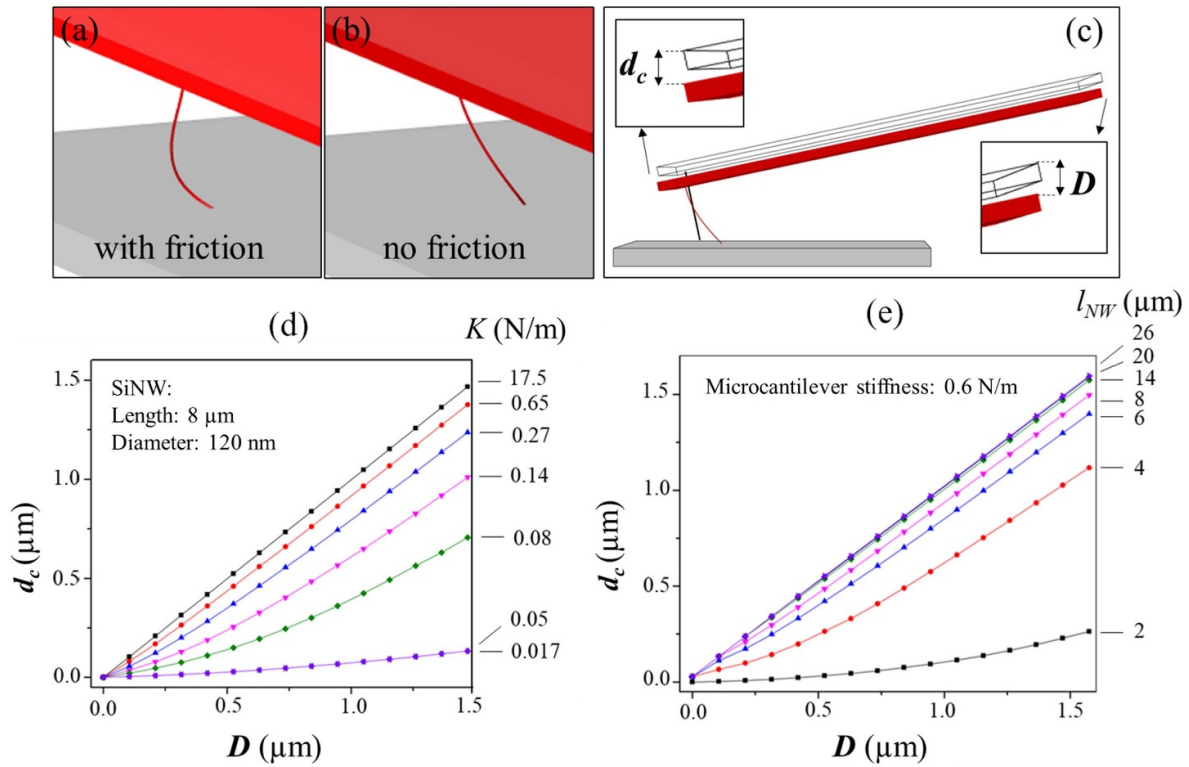


Figure 2. (a) Schematic illustration of a prospective SiNW deformation when the scanning probe is vertically displaced considering friction and no friction, (b) between tip and sample. (c) Illustration of the forced probe displacement D and the achieved microcantilever displacement d_c (d) and (e) microcantilever displacement versus probe displacement for varying microcantilever stiffness K or varying SiNW length l_{NW} (zero-surface-friction approach).

to the mechanical SiNW behavior is the friction interaction between the SiNW tip and the respective sample surface. The friction coefficient determines the degree of SiNW surface sliding in relation to the acting forces during mechanical contact. This aspect is illustrated in figures 2(a) and (b). If the friction coefficient between the sample surface and the SiNW tip is sufficiently high to hold the SiNW in place, the SiNW would tend to buckle. If, on the contrary, the SiNW can slide (assumed here by a so-called zero-surface-friction assumption), the nanowire slides along the surface and bends (figure 2(b)). While we discuss here solely a zero-surface-friction scenario, similar simulations using a friction coefficient of 0.5 are provided in the supplementary information file.

A discussion of the overall tip softness during scanning must however comprise the mechanical microcantilever properties, too (figure 2(c)). As discussed before, the softness of SiNWs is simply due to elastic deformation, e.g. by bending and buckling, once a critical force load is reached during scanning operation. Although, this feature of softness can effectively protect scanned sample surfaces and the tip itself from mechanical deterioration, it can in principle also lower the imaging resolution or obstruct the surface reconstruction. If changes in height are, for instance, tracked by recording the cantilever beam deflection while assuming a stiff tip (e.g. pyramidal shape), buckling or generally elastic deformation of a SiNW tip will consequently falsify the correlation between the surface force and the microcantilever beam deflection. In addition to simple bending and buckling, the

oscillatory behavior must also be taken into account. Based on a microcantilever oscillation, for instance, in non-contact or tapping mode as well as due to the elastic SiNW deformation, further oscillations or eigenfrequencies can be triggered that impair the overall scanning performance. Whether or not an oscillation is excited, depends on both, the SiNW and microcantilever materials as well as the geometric morphology. However, oscillations or eigenfrequencies were not considered further in this study. Generally, microcantilever beams equipped with a soft tip resemble at least a dual spring system. Therefore, also the microcantilever stiffness itself must be taken into account besides the pure SiNW properties. The microcantilever stiffness was systematically varied in our FEM simulation from 0.017 N m^{-1} and 17.5 N m^{-1} (figure 2(d)). Within our FEM simulations, the SiNW length was varied from $2 \mu\text{m}$ to $26 \mu\text{m}$ and the SiNW diameter was set to 120 nm (based on our experiments). By simply comparing a known but forced displacement of the microcantilever, D (maximum $1.5 \mu\text{m}$) and relating it to the actually achieved displacement d_c present at the SiNW-decorated edge (figure 2(c)), the tip softness impact onto a prospective AFM operation can be estimated. In our case, the forced displacement D (cf figure 2(c)) should yield ideally a comparable displacement of the microcantilever tip section if the SiNW behaves as a soft tip. In this case, the tip displacement d_c is ideally equal to D or the relation between d_c and D is linear (figure 2(d)). This is here true for microcantilevers with a spring constant above 0.65 N m^{-1} . Nevertheless, AFM

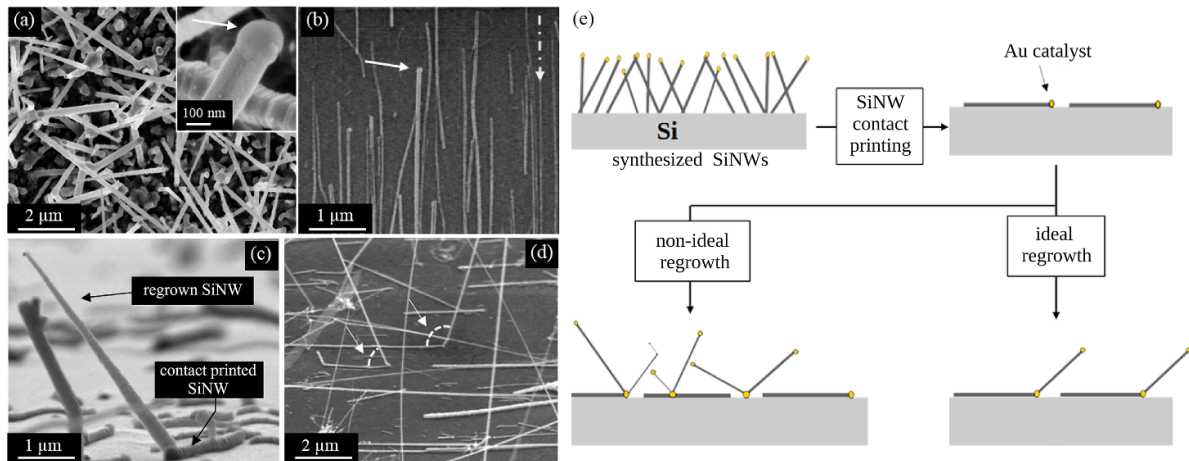


Figure 3. (a) SEM image of synthesized SiNWs on a silicon substrate using gold catalyst. The inset on the right side shows a closer view of a SiNW. The white arrow indicates the gold catalyst at the tip of the wire. (b) Contact printed SiNWs on a silicon substrate; the white dashed arrow shows the direction of CP on the substrate and the solid white arrow indicates the gold catalyst at the tip of the SiNW. (c) SEM image of regrown SiNW (ideal mode) from the tip of a primary contact printed SiNW using the primary growth conditions. (d) SEM image of regrown SiNWs utilizing secondary growth conditions. (e) Schematic illustration of the SiNW regrowth process including SiNW synthesis using a metal catalyst particle, SiNW transfer (here by nanowire CP), and SiNW elongation by reusing the original catalyst. For an ideal regrowth, only a single SiNW is regrown from the catalytic tip of the original SiNW (similar to an ideal SiNW kinking process). The non-ideal modes are mainly inadequate for fabrication of single-SiNW probes.

operation requires a certain microcantilever beam deflection for AFM signal creation. Hence, a compromise must be established between the SiNW and the microcantilever stiffness to enable adequate AFM operation while scanning with a soft tip. The microcantilever stiffness can be readily adjusted, for instance, by the utilized beam length.

The SiNW length can be experimentally changed as well during VLS growth by adapting the total growth time to modify the SiNW stiffness.

The according FEM simulation results are shown in figures 2(d) and (e). Figure 2(e) shows evidently that if the SiNW is shorter than $4\ \mu\text{m}$, based on an assumed diameter of $120\ \text{nm}$, it can hardly be considered as soft anymore. However, above a length of $6\ \mu\text{m}$, the topography image might be increasingly obstructed due to tip softness but only with respect to our set cantilever stiffness of $0.6\ \text{N m}^{-1}$. The fabricated probe depicted in figure 1(d) can consequently be described as a soft tip, which sets it apart from the conventionally employed AFM pyramid-shaped scanning tips and justifies the following experiments.

3. SiNW regrowth principle

As explained in the introduction, regrowth means that a previously VLS-grown nanowire is elongated within a subsequent VLS process. The original idea of the concept was that SiNW kinking and epitaxial growth are possible due to the single crystalline interface between the grown SiNW and the metallic Au-Si catalyst. This would result in controllable spatial angles of the regrown SiNWs.

To grow the initial SiNWs via a VLS mechanism, a nominally $5\ \text{nm}$ thick gold film was at first deposited by thermal evaporation onto single-crystalline silicon (100) wafers that

resemble the so-called growth substrates. The gold film or better the created gold islands or droplets after thermal dewetting during the heating phase of the growth process acted as a metal-catalyst for gold-catalyzed VLS SiNW growth. Further information on the SiNW synthesis is provided in the supplementary information file.

If SiNWs grow from a dewetted metal film, a certain SiNW diameter distribution must be expected. Using colloidal catalyst nanoparticles or by pre-patterning the catalyst, e.g. by nanoimprint lithography [42], diameter control would be immediately gained. The SiNW growth itself was realized in a home-built tube furnace within 60 min at a constant temperature of $550\ ^\circ\text{C}$ and at 10 mbar working pressure using gaseous 2% monosilane (SiH_4) in helium and hydrogen, flowing with 10 sccm and 80 sccm, respectively. In the following, these growth conditions are called ‘primary growth conditions’. The as-synthesized SiNWs are all decorated with a gold-catalyst droplet but randomly oriented on the growth substrate as shown in figure 3(a). The random SiNW orientation is a direct result of the native oxide that is present on the original substrate, thus preventing an epitaxial relation with the nucleated SiNW. The length and diameter of the grown SiNWs are in the range of $5\ \mu\text{m}$ to $8\ \mu\text{m}$ and $10\ \text{nm}$ to $250\ \text{nm}$, respectively. These as-grown SiNWs were subsequently transferred onto a planar silicon substrate covered by native-oxide or to a Si_3N_4 -surface via dry mechanical nanowire CP as illustrated in figure 3(b). A transferred or deposited SiNW with its single catalyst droplet present at its tip confines intrinsically the catalyst area. This localized catalyst droplet (now an Au-Si alloy) was subsequently utilized for a second growth, so-called regrowth, as mentioned before (the catalytic part is indicated by the white arrow in figure 3(b)).

CP allows in principle to control the planar position of single nanowires on a target substrate too by tailored

microtribological features, so-called nanowire catchers [32]. These nanowire catchers must be created prior CP on the substrate by means of further microtechnological procedures. The possibility to define nanowire catchers, e.g. to deposit only single-SiNWs at the bending beam, was here not implemented for simplification reasons but is doable. An example of a photoresist patterning strategy is shown in supplementary information file in figures S2 and S3.

Regrowth of the as-deposited SiNWs was done comparably to the growth of the original SiNWs. However, the catalyst is not pure gold anymore but an eutectic gold–silicon alloy [43]. This aspect is not a critical issue, but a precipitation of excess silicon from the alloy during cool-down at the outer catalyst droplet surface. Surface silicon is prone to oxidation under ambient conditions (native oxide formation) and a native oxide layer is at least partly formed that obstructs potentially a second VLS growth by preventing efficient incorporation of Si from gaseous monosilane within the process. Hence, the native oxide layer was removed using 2% buffered hydrofluoric acid for 10 s as a pretreatment prior to regrowth.

Regrowth relies intrinsically on re-liquefying the VLS catalyst to trigger another SiNW growth. Here, two modes can be discussed. First, the liquid catalyst will wet the original SiNW and the substrate, which leads to an upright but randomly oriented SiNW regrowth. Second, the liquid catalyst droplet adheres solely or predominately to the original SiNW, which could induce a crystal kink [33, 34] at the onset of regrowth. Kinking with an epitaxial interface between the original and the regrown SiNW would be then the basis of controlled SiNW elongation and angular alignment [35]. Within our experiments, transferred SiNWs could be successfully elongated by regrowth.

However, the achieved SiNW growth angles appear currently not aligned to specific kinking directions (figures 3(c) and (d)). In contrary to an ideal epitaxial regrowth, other morphologies or regrowth modes occur as well, which are schematically illustrated in figure 3(e).

The predominant mode is in principle set by the thermodynamic boundary conditions such as SiH₄ partial pressure, working pressure and overall growth temperature. It was for instance observed in comparison with the primary growth conditions that a lower growth temperature of 485 °C, an increased working pressure of 75 mbar, and a higher SiH₄ partial pressure (100 sccm 2% SiH₄ in He, 20 sccm H₂) appeared to increase the likelihood to obtain an ideal regrowth. These growth conditions are called in the following ‘secondary growth conditions’. Regrown SiNWs synthesized under primary growth conditions were typically 5–8 μm long with a diameter of 100–250 nm, whereas by utilizing secondary growth conditions, SiNWs get longer (length about 20–22 μm, increased growth rate) and exhibit smaller diameters (cf figures 3(c) and (d)). The underlying regrowth mechanisms are so far hardly understood but indispensable to further optimize the regrowth in future. Based on our experiments, the orientation of the SiNWs cannot yet be controlled by regrowth, although this was our initial research hypothesis. This aspect therefore hinders currently a high yield of probes as well as

the reproducibility of the fabrication process. The principles of known crystallographic SiNW kinking behavior may still be a key point for controlling SiNW orientations within regrowth in future. Nevertheless, regrown SiNWs at the present state were already suitable to be utilized as a scanning tip in a proof-of-concept manner.

4. SiNW-equipped microcantilever scanning probe fabrication

The fabrication of SiNW-equipped AFM-compatible scanning probes comprises the use or fabrication of a microcantilever as well as the implementation of the aforementioned regrowth of SiNWs. The primary strategy consists of SiNW CP onto suspended membranes that can be subsequently used to fabricate microcantilever beams. The overall principle was already depicted in figure 1(a). For our studies, Si₃N₄-membranes were used as a non-crystalline material that suppresses any epitaxial SiNW growth strategies.

Our microcantilever probes were fabricated from low-stress Si₃N₄-membranes that represent a suitable platform based on their nearly flat surface and their transparency required later for the ease of optical lithography mask alignment. The primary substrates that were used for Si₃N₄-membrane fabrication were commercially available 380 μm thick (100) silicon wafers double-side coated by 1 μm thick low-stress Si₃N₄-films deposited by the low-pressure chemical vapor deposition. The microcantilever fabrication of AFM compatible probes is shown in figure 4 and is in principle compatible to other conventional AFM probe microfabrication procedures (see [44]). First, the membrane and probe body, still held by supporting arms, were defined by positive tone photoresist (AZ5214E) optical lithography and a CF₄-based reactive ion etching (RIE) process to partly remove the Si₃N₄ layer on the backside. After photoresist removal and cleaning (*N*-ethylpyrrolidone, acetone and isopropanol), the unprotected silicon was etched through the entire wafer by using an aqueous solution of KOH (20% wt) at 80 °C (etching rate of approximately 47.5 μm h⁻¹).

The microcantilever beam was fabricated from the remaining front side Si₃N₄-membrane by using again the aforementioned positive tone photoresist optical lithography and CF₄-based RIE. The final AFM compatible probe can be released by breaking the supporting arms by gentle bending and twisting of the probe body. Microcantilevers fabricated in this manner exhibit an initial beam bending of less than 6° with respect to the probe top-surface.

For any implementation of the regrowth principle, it is required to transfer SiNWs from the growth substrate to the microcantilever beam as done here by the aforementioned CP. Within CP, shear forces are the leading forces and enable thus in principle a control of the printed nanowire density by adjusting the normal printing force and shear velocity (here: normal force 0.5 N and shear velocity 1 mm s⁻¹). The most obvious approach is to print SiNWs on the Si₃N₄-membrane, as described before, followed by SiNW regrowth (cf figure 1). CP was realized successfully with the aforementioned parameters

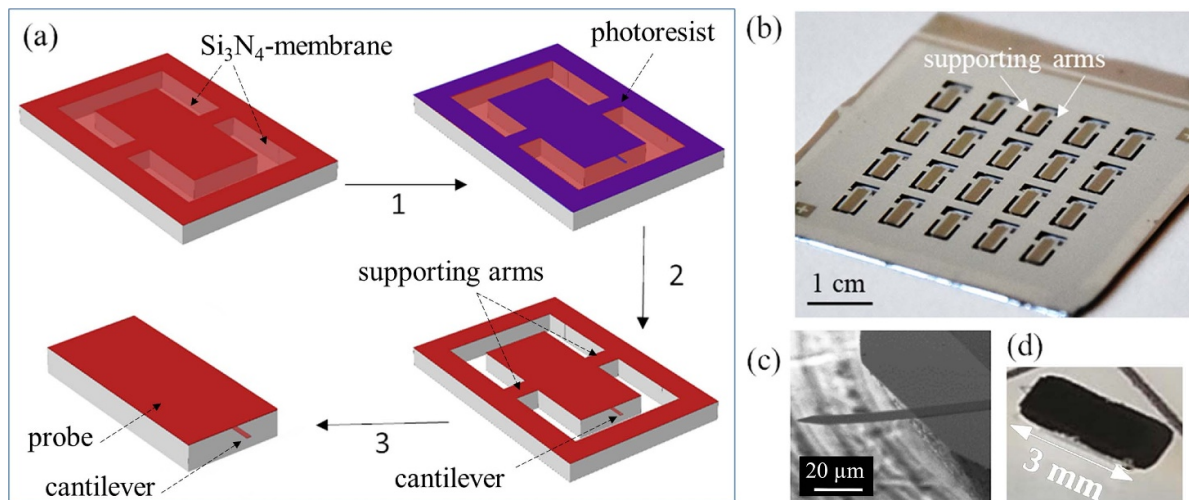


Figure 4. (a) Schematic illustration of cantilever fabrication steps from Si_3N_4 -membranes: (1) photolithography process on a Si_3N_4 -membrane in order to pattern a cantilever area on a photoresist; (2) etching process via RIE technique using CF_4 gas and removing photoresist; (3) fabricated probes are released simply by breaking supporting arms. (b) Fabricated AFM probes; arrows indicate the supporting arms, which can be broken in order to release the probes. (c) and (d) Examples of fabricated probes with single and V-shaped microcantilever beam.

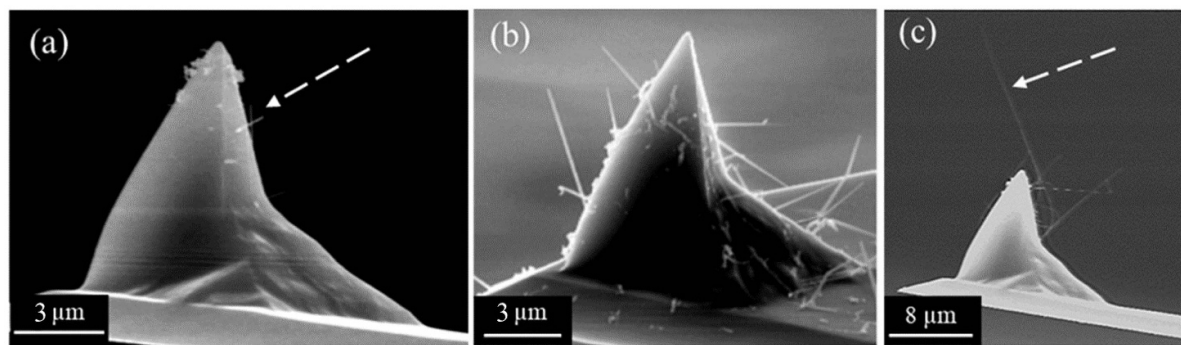


Figure 5. (a) SEM image of contact printed SiNWs on a silicon AFM tip; the white arrow indicates the contact printed SiNWs. (b) SEM image of regrown SiNWs on pyramidal silicon tips using the primary growth conditions. (c) Regrown SiNWs on pyramidal silicon tips using our secondary growth conditions (SEM image).

and without any observable breakage of the suspended membranes. Nevertheless, the most straightforward strategy is to print SiNWs directly on free-standing, tip-less microcantilever beams, which worked surprisingly well without any damage by precisely controlling the applied force (see supplementary information file for details).

The use of commercially available tip-less microcantilevers as a substrate material is intriguing because it omits any need to establish an own microcantilever fabrication. However, the implementation of CP catchers is challenging or requires at least further process steps [45]. Based on the promising results achieved on tip-less microcantilevers, also commercial AFM cantilevers equipped with the well-known pyramidal tips were utilized ($2 \mu\text{m}$ thick Si microcantilevers, stiffness 0.1 N m^{-1}). Notably, the pyramidal tip acted as a kind of nanowire catcher (figure 5(a)) and allowed to decorate the pyramidal tip with SiNWs (figures 5(b) and (c)). Some commercial pyramidal tips were even decorated accidentally with exposed single-SiNWs that sufficed, although poorly, as a SiNW AFM scanning tip (figure 5(d)) as discussed later.

5. Regrown SiNWs as AFM scanning probes for topography reconstruction

A critical parameter for AFM measurements, currently not controllable for the regrowth process, is the reproducibility of the polar but even more of the azimuthal angle of the regrown SiNWs. But post-alignment of SiNWs is generally possible and can be achieved, for instance, by focused ion-beam alignment as reported elsewhere [10]. Due to the angular alignment of SiNWs, AFM image artifacts were expected to depend on the SiNWs polar angle, the azimuthal angle, the sample topography and the scanning direction and mode. In order to investigate this aspect and in particular the overall functionality of regrown SiNW tips, AFM measurements were done using a specified reference sample composed of a SiO_2 -based array of circular pillars (pillar diameter of $2.6 \mu\text{m}$, pillar height of 500 nm , and pitch size of $5 \mu\text{m}$).

AFM measurements using regrown SiNWs situated on the pyramidal tip of commercial AFM probes (cf figure 5(c)) could be only realized in the so-called contact mode as shown

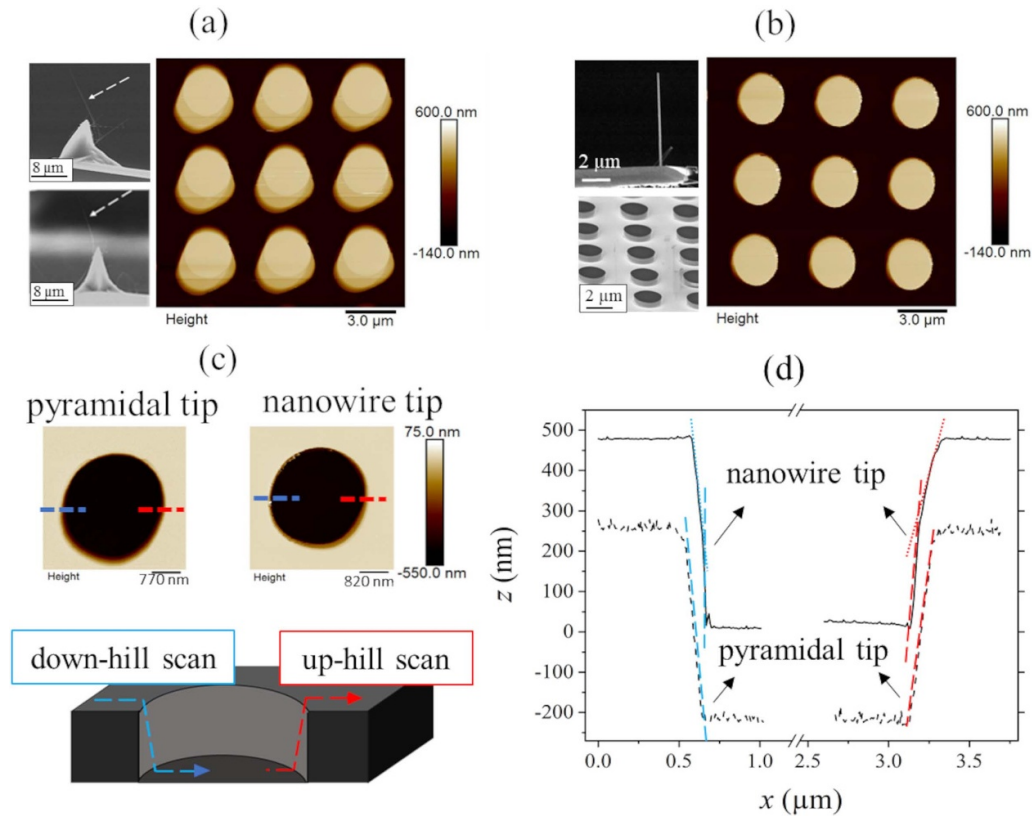


Figure 6. (a) SEM images of a SiNW scanning tip situated on a silicon pyramid and AFM topography image of the reference (right). The upper and lower images (left) depict the same SiNW grown on a pyramidal tip inside- and front-view. (b) SEM images of a regrown SiNW probe on a Si₃N₄-microcantilever (top-left) and SEM image of the reference sample (lower left) as well as AFM topography image of the reference sample (right). (c) Indicated line scans on the reference sample decorated with pits (top) for the probes shown in (a) conventional pyramidal silicon tip and the probe shown in (b) as well as an illustration of the overall scan scenario. (d) Line profiles as indicated in (c) to evaluate the high aspect ratio properties of the scanning tips.

in figure 6(a). The circular pillars appear, for instance, well-resolved in the upper half but the lower half of the structures are distorted by tip artifacts. In fact, this asymmetry can be explained by the azimuthal angle of the SiNW that creates asymmetric scanning conditions. These SiNW tips appeared generally inappropriate for an AFM scanning operation based on the distorted topography images. Such SiNW tips showed furthermore clear signs of wear such as adhesion loss to the pyramidal substrate tip, breakage and failed thus frequently. However, the use of such tips is not intrinsically limited by the overall geometric SiNW conditions unless elastic deformation is discussed, as has already been done using our aforementioned simulations. The performance of such tips is however, not discussed any further (see supplementary information file).

SiNWs that were regrown on Si₃N₄-microcantilevers gave in contrary well-resolved topography images of the utilized reference sample as shown in figure 6(b) and enabled furthermore, a usage of the so-called AFM peak-force tapping mode. The pitch and height of the structures are here in alignment with the reference sample specifications. The SiNW tips remained for almost all cases intact despite multiple use and survived even high loads of up to 90 nN while using hard sample surfaces represented here by sapphire (see supplementary information file).

In order to compare the functionality of SiNW tips with common pyramidal silicon tips (conventional AFM probe, Bruker-OTESPA, with spring constant of 14 N m^{-1} and resonant frequency of 210 kHz), topography measurements were performed using the same conditions on the reference sample (air, contact mode). The measurements yielded comparable results with a pillar height of 476 nm (error about 5% compared to reference) and 468 nm (error 6%) for the commercial and the SiNW tip, respectively. The measured root-mean-square roughness values using the peak-force tapping mode on the silicon surface between the pillars by a SiNW tip and a plain silicon pyramidal tip are $(1.81 \pm 0.01) \text{ nm}$ and $(8.4 \pm 0.4) \text{ nm}$, respectively.

The fact that silicon AFM pyramidal tips exhibit a smaller tip radius (nearly 10 nm, based on specifications) compared to the SiNW tip with a tip radius in the range of 60 nm, yields consequently an increased lateral resolution of the pyramidal silicon tip. Hence, the SiNW scanning tip is more prone to smoothing (cf supplementary information file). Nevertheless, the SiNW tip can be sharpened too by adequate post-processing as, for instance, discussed briefly as well in the supplementary information file. Generally, this gold-based particle is considered to have lower wear resistance compared to silicon or silicon oxide. Therefore, removing the catalyst can be a simple solution to increase the wear resistance of

these scanning tips. The Au–Si alloy particles can be, for instance, etched in a potassium iodide solution (see supplementary information). However, post-sharpening of the tip may still be required to achieve or approach the tip radius of conventional pyramidal tips. However, as previously stated, the hemispherical catalyst on the SiNW tip still has a high potential, e.g. for use in the examination of soft and delicate surfaces. To evaluate the performance of SiNW probes further, comparative measurements using conventional AFM cantilevers and a reference sample with circular pit structures instead of pillars but with the same diameter, pitch size and height as the aforementioned reference sample were done. The overall topography scan appears rather similar, although slightly improved for SiNW tips, and exhibits even similar scan asymmetry artifacts as shown in figure 6(c). To improve the analysis, the transition from the surface to the pit bottom was furthermore, inspected as indicated and illustrated in figure 6(c). The transition slope can here serve as a first performance indicator that is created by convolution of the real surface profile, assumed as vertical sidewall, with the tip geometry. As shown in figure 6(d), the pyramidal tip shows at first, as expected, an almost ideal linear transition behavior with a slope of about -3.9 ± 0.1 and 3.1 ± 0.1 for down and up scanning, respectively. Notably, lower slopes are obtained for up scans, which should be due to the observed scan asymmetry for both, pyramidal and SiNW tips (cf figure 6(c)).

The description of the SiNW scanning tip behavior requires in contrary, two regions as indicated in figure 6(d). We currently believe that the upper region or slope is most likely attributed to the larger tip radius of SiNW scanning tip as well as to the SiNW alignment while the lower region is attributed to the SiNW high aspect ratio geometry. If both regions are described in a first order approximation by a linear trend, a slope for the upper part of about -3.8 ± 0.8 and 1.8 ± 0.1 , and for the lower part of about -9.3 ± 0.1 and 4.7 ± 0.3 always for down and up scanning, respectively is obtained.

This result provides an experimental indication of an improved suitability of SiNW scanning tips to measure high aspect ratio geometries based on the increased sloped in the lower part in comparison the conventional pyramidal scanning tip. Besides, from pure topological surface reconstructions, the utilized peak-force tapping mode has the inherent advantage that along with the topography also mechanical properties of the sample can be determined. The tip approach and retraction behavior is here important and can be extracted from so-called force graphs available for each scanned point (cf supplementary information file). The minimum force observed in the retract graph indicates the adhesion force between the tip and the sample [46].

The retract plot of a SiNW tip is compared accordingly again with the pyramidal tip but this time on a sapphire sample. The peak-force value was kept constant for both tips at 75 nN. The adhesion force is estimated for the pyramidal silicon tip with around 36 nN and for the SiNW tip with 50 nN. Notably, both values are in overall agreement and support the usability of our SiNW tips. The slight difference could be due to the presence of the gold–silicon alloy catalyst that was still present at the SiNW tip.

The experimental results indicate clearly that regrown SiNW tips suffice to create AFM soft scanning probes. In this regard, the superior durability can be as well emphasized. Nevertheless, a broader usability is currently limited by the low reproducibility of the regrowth process, which comprises lack of angular SiNW orientation control as well as the control over the overall regrowth yield. If adequate regrowth conditions can be established, this method might be a capable strategy for nanowire-equipped AFM scanning probes even beyond silicon.

6. Conclusion

We presented a strategy to equip microcantilever beams with single-SiNW scanning tips that were directly grown by gold-catalyzed VLS synthesis. We discussed the SiNW tip softness and the impact of the microcantilever stiffness based on FEM simulations. The overall assembly strategy relies on so-called SiNW regrowth, which comprises a SiNW elongation from previously transferred, as-grown SiNW, e.g. by nanowire CP, and reusing the original growth gold catalyst within a second VLS growth process. The regrowth process requires still further research to increase the overall reproducibility and yield as well as to enable control over the polar and azimuthal angular alignment of regrown SiNWs. Nevertheless, SiNW scanning probes were successfully created in this manner on Si_3N_4 microcantilevers and implemented for AFM.

AFM measurements showed evidently that the assembled SiNW scanning tips are suitable for topography reconstruction as well as overall comparable with conventional pyramidal scanning tips besides their high aspect-ratio nature and a superior durability.



Data availability statement

All data that support the findings of this study are included within the article (and any supplementary files).

Acknowledgments

We gratefully acknowledge the financial support by the German Federal Ministry of Education and Research (BMBF, NanoMatFutur 13N12545) and by the German Research Foundation (DFG 392124230) as well as the experimental support by S Jenisch and A Minkow (Ulm University).

ORCID iDs

M Nilsen  <https://orcid.org/0000-0003-3035-4718>
S Strehle  <https://orcid.org/0000-0002-1261-2894>

References

- [1] Ruxandra V, Quinlan F T and Stroeve P 2002 Use of *in situ* electrochemical atomic force microscopy (EC-AFM) to monitor cathode surface reaction in organic electrolyte *Ind. Eng. Chem. Res.* **41** 6546–54

- [2] Göken M and Kempf M 1999 Microstructural properties of superalloys investigated by nanoindentations in an atomic force microscope *Acta Mater.* **47** 1043–52
- [3] Westra K L and Thomson D J 1995 The microstructure of thin films observed using atomic force microscopy *Thin Solid Films* **257** 15–21
- [4] Argaman M, Golan R, Thomson N H and Hansma H G 1997 Phase imaging of moving DNA molecules and DNA molecules replicated in the atomic force microscope *Nucleic Acids Res.* **25** 4379–84
- [5] Gross L, Mohn F, Moll N, Liljeroth P and Meyer G 2009 The chemical structure of a molecule resolved by atomic force microscopy *Science* **325** 1110–4
- [6] Cappella B and Dietler G 1999 Force-distance curves by atomic force microscopy *Surf. Sci. Rep.* **34** 1–104
- [7] Cumpson P J, Clifford C A, Portoles J F, Johnstone J E and Munz M 2008 Cantilever spring-constant calibration in atomic force microscopy *Applied Scanning Probe Methods VIII* (Berlin: Springer) pp 289–314
- [8] Martínez L, Tello M, Díaz M, Román E, Garcia R and Huttel Y 2011 Aspect-ratio and lateral-resolution enhancement in force microscopy by attaching nanoclusters generated by an ion cluster source at the end of a silicon tip *Rev. Sci. Instrum.* **82** 023710
- [9] Bryce B A, Ilic B R, Reuter M C and Tiwari S 2014 Wafer scale tilt-compensated silicon nanowire atomic force microscopy probes for high aspect ratio geometries *J. Micromech. Microeng.* **24** 095016
- [10] Knittel P, Hibst N, Mizaikoff B, Strehle S and Kranz C 2017 Focused ion beam-assisted fabrication of soft high-aspect ratio silicon nanowire atomic force microscopy probes *Ultramicroscopy* **179** 24–32
- [11] Nguyen C V, Chao K-J, Stevens R M D, Delzeit L, Cassell A, Han J and Meyyappan M 2001 Carbon nanotube tip probes: stability and lateral resolution in scanning probe microscopy and application to surface science in semiconductors *Nanotechnology* **12** 363–7
- [12] Tan S C, Zhao H and Thompson C V 2016 Fabrication of high aspect ratio AFM probes with different materials inspired by TEM ‘lift-out’ method *J. Vac. Sci. Technol. B* **34** 051805
- [13] Wilson N R and Macpherson J V 2009 Carbon nanotube tips for atomic force microscopy *Nat. Nanotechnol.* **4** 483–91
- [14] Engstrom D S, Savu V, Zhu X, Bu I Y Y, Milne W I, Brugger J and Boggild P 2011 High throughput nanofabrication of silicon nanowire and carbon nanotube tips on AFM probes by stencil-deposited catalysts *Nano Lett.* **11** 1568–74
- [15] Chen J 2014 Nanobiomechanics of living cells: a review *Interface Focus* **4** 20130055
- [16] Ren B, Picardi G and Pettinger B 2004 Preparation of gold tips suitable for tip-enhanced Raman spectroscopy and light emission by electrochemical etching *Rev. Sci. Instrum.* **75** 837–41
- [17] Kalkbrenner T, Ramstein M, Mlynek J and Sandoghdar V 2001 A single gold particle as a probe for apertureless scanning near-field optical microscopy *J. Microsc.* **202** 72–6
- [18] Christiansen S H, Becker M, Fahlbusch S, Michler J, Sivakov V, Andrä G and Geiger R 2007 Signal enhancement in nano-Raman spectroscopy by gold caps on silicon nanowires obtained by vapour–liquid–solid growth *Nanotechnology* **18** 035503
- [19] Hobbs R G, Petkov N and Holmes J D 2012 Semiconductor nanowire fabrication by bottom-up and top-down paradigms *Chem. Mater.* **24** 1975–91
- [20] Mikolajick T, Heinzig A, Trommer J, Pregl S, Grube M, Cuniberti G and Weber W M 2013 Silicon nanowires—a versatile technology platform *Phys. Status Solidi Rapid Res. Lett.* **7** 793–9
- [21] Schmidt V, Wittemann J V, Senz S and Gösele U 2009 Silicon nanowires: a review on aspects of their growth and their electrical properties *Adv. Mater.* **21** 2681–702
- [22] Schmidt V, Wittemann J V and Gösele U 2010 Growth, thermodynamics, and electrical properties of silicon nanowires[†] *Chem. Rev.* **110** 361–88
- [23] Wagner R S and Ellis W C 1964 Vapor–liquid–solid mechanism of single crystal growth *Appl. Phys. Lett.* **4** 89–90
- [24] Ramanujam J, Shiri D and Verma A 2011 Silicon nanowire growth and properties: a review *Mater. Express* **1** 105–26
- [25] Whang S J, Lee S J, Yang W F, Cho B J, Liew Y F and Kwong D L 2007 Complementary Al-catalyzed silicon nanowires *Electrochem. Solid-State Lett.* **10** E11
- [26] Wittemann J V, Münchgesang W, Senz S and Schmidt V 2010 Silver catalyzed ultrathin silicon nanowires grown by low-temperature chemical-vapor-deposition *J. Appl. Phys.* **107** 096105
- [27] Hasan M, Huq M F and Mahmood Z H 2013 A review on electronic and optical properties of silicon nanowire and its different growth techniques *Springerplus* **2** 151
- [28] Björk M T, Knoch J, Schmid H, Riel H and Riess W 2008 Silicon nanowire tunneling field-effect transistors *Appl. Phys. Lett.* **92** 193504
- [29] Behroudj A, Geiger D and Strehle S 2019 Epitaxial bottom-up growth of silicon nanowires on oxidized silicon by alloy-catalyzed gas-phase synthesis *Nano Lett.* **19** 7895–900
- [30] Thalluri S M et al 2018 Highly-ordered silicon nanowire arrays for photoelectrochemical hydrogen evolution: an investigation on the effect of wire diameter, length and inter-wire spacing *Sustain. Energy Fuels* **2** 978–82
- [31] Llobet J, Rius G, Chuquitarqui A, Borrisé X, Kooops R, Van Veghel M and Perez-Murano F 2018 Arrays of suspended silicon nanowires defined by ion beam implantation: mechanical coupling and combination with CMOS technology *Nanotechnology* **29** 155303
- [32] Roßkopf D and Strehle S 2016 Surface-controlled contact printing for nanowire device fabrication on a large scale *Nanotechnology* **27** 185301
- [33] Wagner R S and Ooherty C J 1968 Mechanism of branching and kinking during VLS crystal growth *J. Electrochem. Soc.* **115** 93
- [34] Westwater J, Gosain D P, Tomiya S, Usui S and Ruda H 1997 Growth of silicon nanowires via gold/silane vapor–liquid–solid reaction *J. Vac. Sci. Technol. B* **15** 554
- [35] He Z, Nguyen H T, Duc Toan L and Pribat D 2015 A detailed study of kinking in indium-catalyzed silicon nanowires *CrystEngComm* **17** 6286–96
- [36] Zhu Y, Xu F, Qin Q, Fung W Y and Lu W 2009 Mechanical properties of vapor–liquid–solid synthesized silicon nanowires *Nano Lett.* **9** 3934–9
- [37] Sadeghian H, Yang C K, Goosen J F L, Van Der Drift E, Bossche A, French P J and Van Keulen F 2009 Characterizing size-dependent effective elastic modulus of silicon nanocantilevers using electrostatic pull-in instability *Appl. Phys. Lett.* **94** 221903
- [38] Lee B and Rudd R E 2007 First-principles calculation of mechanical properties of Si(001) nanowires and comparison to nanomechanical theory *Phys. Rev. B* **75** 195328
- [39] Li X, Ono T, Wang Y and Esashi M 2003 Ultrathin single-crystalline-silicon cantilever resonators: fabrication technology and significant specimen size effect on Young’s modulus *Appl. Phys. Lett.* **83** 3081–3
- [40] Gordon M J, Baron T, Dhalluin F, Gentile P and Ferret P 2009 Size effects in mechanical deformation and fracture of cantilevered silicon nanowires *Nano Lett.* **9** 525–9

- [41] Heidelberg A, Ngo L T, Wu B, Phillips M A, Sharma S, Kamins T I, Sader J E and Boland J J 2006 A generalized description of the elastic properties of nanowires *Nano Lett.* **6** 1101–6
- [42] Wang C, Murphy P F, Yao N, McIlwrath K and Chou S Y 2011 Growth of straight silicon nanowires on amorphous substrates with uniform diameter, length, orientation, and location using nanopatterned host-mediated catalyst *Nano Lett.* **11** 5247–51
- [43] Okamoto H and Massalski T B 1983 The Au–Si (Gold-Silicon) system *Bull. Alloy Phase Diagr.* **4** 190–8
- [44] Schürmann G, Noell W, Stauffer U, De Rooij N F, Eckert R, Freyland J M and Heinzelmann H 2001 Fabrication and characterization of a silicon cantilever probe with an integrated quartz-glass (fused-silica) tip for scanning near-field optical microscopy *Appl. Opt.* **40** 5040
- [45] Nilsen M, Port F, Roos M, Gottschalk K-E and Strehle S 2019 Facile modification of freestanding silicon nitride microcantilever beams by dry film photoresist lithography *J. Micromech. Microeng.* **29** 025014
- [46] Pittenger B, Erina N and Su C 2014 Mechanical property mapping at the nanoscale using peakforce QNM scanning probe technique pp 31–51